Title

The inner membrane complex sub-compartment proteins critical for replication of the apicomplexan parasite Toxoplasma gondii adopt a pleckstrin homology fold.

Journal

Journal of Biological Chemistry, 289(20)

Authors

Tonkin, Michelle
Beck, Josh
Bradley, Peter
et al.

Publication Date

2014-05-16

DOI

10.1074/jbc.M114.548891

Peer reviewed

THE JOURNAL OF BIOLOGICAL CHEMISTRY VOL. 289, NO. 20, pp. 13962–13973, May 16, 2014

The Inner Membrane Complex Sub-compartment Proteins Critical for Replication of the Apicomplexan Parasite *Toxoplasma gondii* Adopt a Pleckstrin Homology Fold*

Received for publication, January 8, 2014, and in revised form, March 18, 2014 Published, JBC Papers in Press, March 27, 2014, DOI 10.1074/jbc.M114.548891

Michelle L. Tonkin[‡1], **Josh R. Beck**[§], **Peter J. Bradley**[§], **and Martin J. Boulanger**[‡2]

From the [‡]*Department of Biochemistry and Microbiology, University of Victoria, Victoria, British Columbia V8W 3P6, Canada and* [§]*Department of Microbiology, Immunology, and Molecular Genetics, UCLA, Los Angeles, California 90095*

Background: Inner membrane complex sub-compartment Proteins (ISPs) are critical for proper cell division of apicomplexan parasites, but the mechanism is unknown.
Results: ISPs adopt a pleckstrin homology (PH)-fold yet do not retain phospholipid-binding activity.
Conclusion: ISPs appear to repurpose the phospholipid-binding site to recruit protein partners.
Significance: First structural characterization of an ISP from any organism.

Toxoplasma gondii*, an apicomplexan parasite prevalent in developed nations, infects up to one-third of the human population. The success of this parasite depends on several unique structures including an inner membrane complex (IMC) that lines the interior of the plasma membrane and contains proteins important for gliding motility and replication. Of these proteins, the IMC sub-compartment proteins (ISPs) have recently been shown to play a role in asexual *T. gondii* daughter cell formation, yet the mechanism is unknown. Complicating mechanistic characterization of the ISPs is a lack of sequence identity with proteins of known structure or function. In support of elucidating the function of ISPs, we first determined the crystal structures of representative members *Tg*ISP1 and *Tg*ISP3 to a resolution of 2.10 and 2.32 Å, respectively. Structural analysis revealed that both ISPs adopt a pleckstrin homology fold often associated with phospholipid binding or protein-protein interactions. Substitution of basic for hydrophobic residues in the region that overlays with phospholipid binding in related pleckstrin homology domains, however, suggests that ISPs do not retain phospholipid binding activity. Consistent with this observation, biochemical assays revealed no phospholipid binding activity. Interestingly, mapping of conserved surface residues combined with crystal packing analysis indicates that *Tg*ISPs have functionally repurposed the phospholipid-binding site likely to coordinate protein partners. Recruitment of larger protein complexes may also be aided through avidity-enhanced interactions resulting from multimerization of the ISPs. Overall, we propose a model where *Tg*ISPs recruit protein partners to the IMC to ensure correct progression of daughter cell formation.

The phylum Apicomplexa contains >5000 obligate intracellular parasitic protozoans that cause devastating diseases on a global scale. Two of the major pathogens in this phylum are *Plasmodium* spp., the causative agents of malaria that are responsible for more than one million human deaths per annum (1), and *Toxoplasma gondii*, the etiological agent of toxoplasmosis, a widespread disease particularly affecting immune-compromised patients and congenitally infected neonates (2). The success of these parasites is largely due to various phylum-specific biological processes, cellular structures, and proteins that hold intriguing promise as therapeutic targets. The inner membrane complex (IMC)[3] is an apicomplexan-specific structure that consists of an intricate system of flattened vesicles and associated filamentous network underlying the parasite plasma membrane (3–6). This patchwork of membrane sacs consists of rectangular plates around the center and bottom of the parasite, capped by a single conical apical plate, with openings at the apex and base of the cell (3). The IMC is a critical anchor point for gliding motility, a type of movement unique to apicomplexans that may be required for host cell invasion, and also serves as a scaffold for proper daughter cell formation (7, 8). The limited number of proteins known to associate directly with the IMC (9–13) combined with the importance of the IMC to parasite invasion and replication prompted our recent identification and characterization of a new family of IMC associated proteins (14).

Three proteins were initially identified and found to localize to distinct sub-compartments of the IMC in *T. gondii*: IMC sub-compartment protein (ISP) 1, ISP2, and ISP3 (14). The ISP family appears to be conserved throughout *Apicomplexa*, suggesting that these proteins are critical factors in parasite viability. In support of this notion, disruption of *Tg*ISP2 caused a

* This work was supported by Canadian Institutes for Health Research Grant MOP82915 (to M. J. B.), a National Institutes of Health Microbial Pathogenesis Training Grant T32 AI07323 (to J. R. B.), and Grant RO1 AI064616 (to P. J. B.).

The atomic coordinates and structure factors (codes 4CHM and 4CHJ) have been deposited in the Protein Data Bank (http://wwpdb.org/).

[1] Supported by a Natural Sciences and Engineering Research Council of Canada Alexander Graham Bell Canada Graduate Scholarship (CGSD3) and a Ventura Neale Trust Endowed PEO Scholar Award.

[2] A Canadian Institutes for Health Research New Investigator, a Michael Smith Foundation for Health Research scholar, and a Canada Research Chair. To whom correspondence should be addressed: Dept. of Biochemistry and Microbiology, University of Victoria, P. O. Box 3055 STN CSC, Victoria, BC, Canada V8W 3P6. Tel.: 250-721-7072; Fax: 250-721-8855; E-mail: mboulang@uvic.ca.

[3] The abbreviations used are: IMC, inner membrane complex; AU, asymmetric unit; IP, inositol phosphates; ISP, IMC sub-compartment protein; PH, pleckstrin homology; SeMet, selenomethionine.

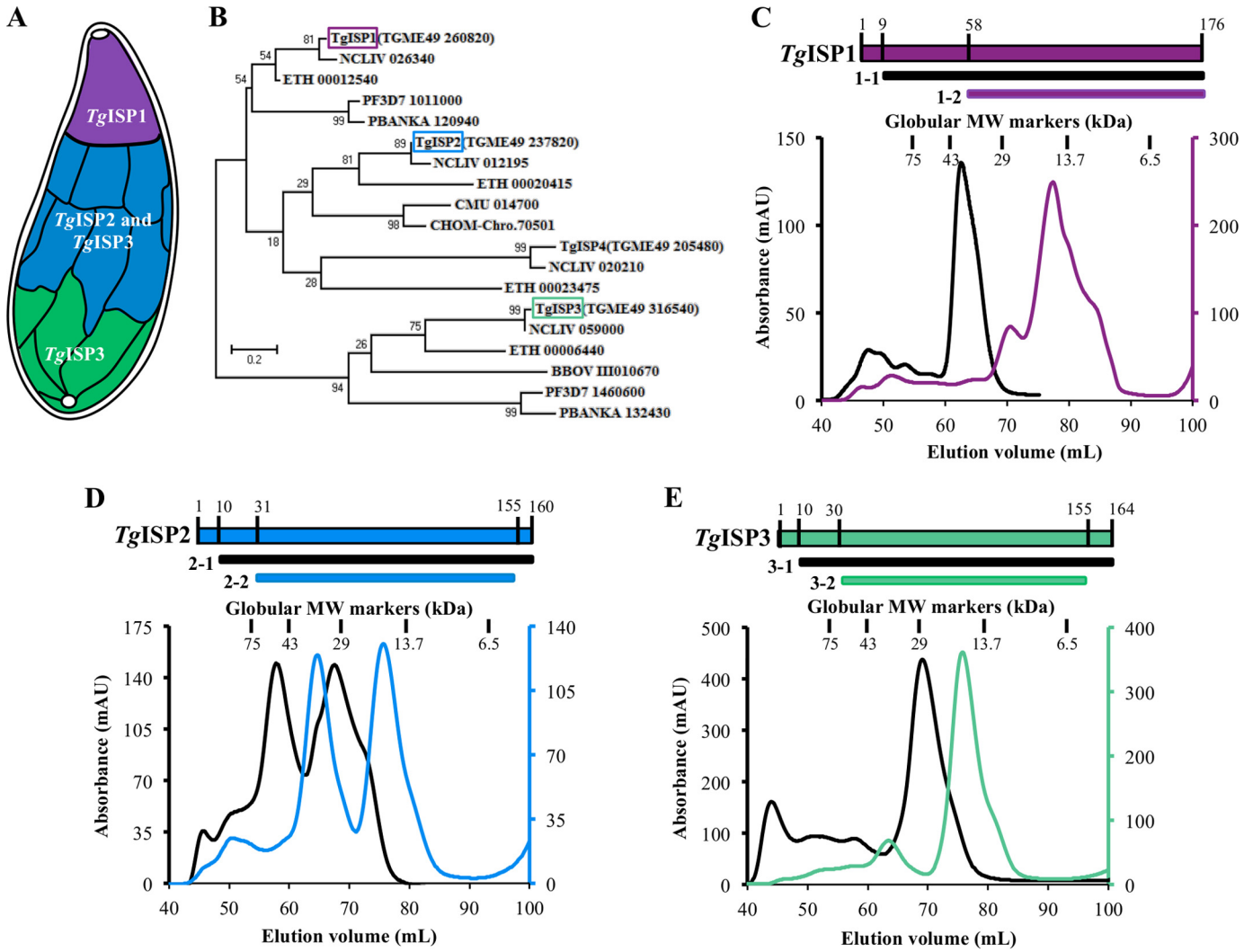

FIGURE 1. **Construct design and gel filtration profiles for *Tg*ISPs from both apicomplexan ISP clades show complex molecular organization.** *A*, schematic of the distribution of ISPs along the IMC of *T. gondii* (adapted from Ref 14). *B*, phylogenetic analysis of apicomplexan ISPs shows a bifurcated clustering with either *Tg*ISP1/ISP2 or *Tg*ISP3. *C*, *top*, two constructs were subcloned for characterization of *Tg*ISP1: *Tg*ISP1-1 and *Tg*ISP1-2. *Bottom*, size exclusion chromatograms for *Tg*ISP1-1 (*black line*, 19.5 kDa) and *Tg*ISP1-2 (*purple line*; 13.9 kDa) from a Superdex75 16/60 column. *Vertical lines* represent the peak centers for a set of globular standards. *D*, *top*, *Tg*ISP2: *Tg*ISP2-1 and *Tg*ISP2–2. *Bottom*, size exclusion chromatograms for *Tg*ISP2-1 (*black line*; 17.3 kDa), *Tg*ISP2–2 (*blue line*, 14.5 kDa). *E*, *top*, *Tg*ISP3: *Tg*ISP3-1, *Tg*ISP3-2. *Bottom*, size exclusion chromatograms for *Tg*ISP3-1 (*black line*; 18.3 kDa), *Tg*ISP3-2 (*green line*, 15.0 kDa).

significant loss in parasite fitness and a severe defect in endodyogeny (14), the form of internal cell budding in which two daughter cells are formed within the intact mother parasite. In particular, parasites lacking ISP2 generate abnormal numbers of daughter cells during endodyogeny. All three *Tg*ISP proteins contain N-terminal cysteine and glycine residues required for targeting to the IMC membranes by palmitoylation and myristoylation, respectively (14). The *Tg*ISP proteins are organized in a hierarchical manner through an unknown mechanism, with *Tg*ISP1 localizing exclusively to the conical apical plate, *Tg*ISP2 localizing to the IMC sub-compartment that begins after the apical cap and extends approximately two-thirds down the length of the parasite, and *Tg*ISP3 localizing to the same region as *Tg*ISP2 in addition to the basal end of the IMC (Fig. 1*A*). This organization is increasingly complex, as a genetic knock-out of *Tg*ISP1 revealed a gate-keeping function; in the absence of TgISP1, *Tg*ISP2 and *Tg*ISP3 were re-localized to the apical IMC cap.

A fourth member of the ISP family in *T. gondii* was more recently identified; *Tg*ISP4 localizes to the same sub-compartment as *Tg*ISP2 but is distinct in that it appears to only require palmitoylation for membrane association. *Tg*ISP4 has lower expression levels than the other family members and a different expression timing through the cell cycle. Disruption of *Tg*ISP4 did not show any defects in cell growth or replication, but whether or not redundancy plays a role in ISP function is currently unknown (15).

The ISPs have also recently been characterized in *Plasmodium berghei*, which only contains two family members, ISP1 and ISP3, and both were found to be important for defining apical polarity (16). Although each of the ISPs can be disrupted in *T. gondii*, only ISP3 knockouts could be obtained in *P. berghei*, suggesting that ISP1 may be essential. Interestingly, the localization of ISP1 is altered in Δ*isp3* parasites, indicating these proteins act in a coordinated fashion similar to the *Tg*ISPs.

Although the importance of ISPs is clear, the detailed function of these proteins remains elusive. Complicating their functional assignment is the lack of sequence homology to characterized domains or folds. Using a phylogenetic analysis we initially show that the apicomplexan ISPs are divided into two distinct clades. We then used x-ray crystallography to characterize the three-dimensional structures of *Tg*ISP1 and *Tg*ISP3, representatives of the two phylogenetic clades. Intriguingly, both structures adopt a pleckstrin homology (PH) fold often found to support protein-lipid or protein-protein interactions. Collectively, these first structures of an ISP offer insight into possible mechanisms by which the ISPs enable correct daughter cell formation.

EXPERIMENTAL PROCEDURES

Bioinformatics

Select high confidence apicomplexan ISP sequences were obtained from UniProt, NCBI, and OrthoMCL database searches combined with our previous identification of ISP paralogs and orthologs (14), aligned with MUSCLE (17), and used to generate a maximum likelihood phylogenetic tree tested with 500 bootstrap replicates in MEGA6.0 (18).

For conservation mapping with ConSurf (19), complete or partial apicomplexan ISP sequences were aligned with MUSCLE (17) and mapped onto the *Tg*ISP1 core (trimmed to remove ordered expression tag sequences).

Construct Design and Cloning

The genes encoding ISP1 (TGME49_260820), ISP2 (TGME49_237820), and ISP3 (TGME49_316540) were amplified from *T. gondii* type II cDNA and cloned NheI-NotI into a pET28a vector modified to contain an N-terminal hexahistidine tag separated from the ISP sequence by either a tobacco etch virus protease or thrombin cleavage site. Sequence analysis confirmed that no mutations were introduced during amplification procedures.

TgISP1—Two constructs of *Tg*ISP1 were further cloned for functional studies and crystallization trials as described previously (20): *Tg*ISP1-1 (post N-terminal localization residues (Gly-2, Cys-8, Cys-9) to C terminus; Ala-9 to Ala-176) and *Tg*ISP1-2 (conserved core; Pro-58 to Ala-176).

TgISP2—Two constructs of *Tg*ISP2 were subcloned for functional studies and crystallization trials. *Tg*ISP2-1 extends from Gly-10 after the N-terminal residues involved in localization (Gly-2, Cys-5, Cys-8, and Cys-9) to Ala-160 at the C terminus of the protein. *Tg*ISP2–2 extends from Ser-31 to Ala-155 (conserved core).

TgISP3—Two constructs of *Tg*ISP3 were subcloned for functional studies and crystallization trials. *Tg*ISP3-1 extends from Asp-10 after the N-terminal residues involved in localization (Gly-2, Cys-6, Cys-7) to Asn-164 at the C terminus of the protein. *Tg*ISP3-2 extends from Pro-30 to Asn-155 (conserved core).

Protein Expression and Purification

All constructs of the three *Tg*ISP proteins were produced recombinantly in *E. coli* BL21-CodonPlus cells (Stratagene) and purified by nickel-affinity and size exclusion chromatography as described previously for *Tg*ISP1-2 (20), with the following exceptions; *Tg*ISP1-1, *Tg*ISP2-1, and *Tg*ISP3-1 contained an N-terminal thrombin cleavage site, and after nickel-affinity purification the proteins were buffer-exchanged into HEPES-buffered saline (20 mM HEPES, pH 7.0, 150 mM NaCl) containing 1 mM DTT or β-mercaptoethanol and 2.25 mM $CaCl_2$ and cleaved with thrombin by overnight incubation at 18 °C.

A selenomethionine (SeMet) version of *Tg*ISP1-2 (*Tg*ISP1-2_SeMet) was generated by transforming the clone into the methionine auxotroph *E. coli* 834 strain and inoculating SeMet media (Molecular Dimensions) containing 50 μg/ml ampicillin. The culture was grown at 37 °C to an A_{600} of 0.9 and induced with 1 mM isopropyl 1-thio-β-D-galactopyranoside. After 12 h of growth at 30 °C, the cells were harvested by centrifugation, and the SeMet-labeled protein was purified using the same protocol as for the native protein (20).

The purity of each protein was assessed at every stage by SDS-PAGE, and protein concentrations were determined by the Bradford assay for *Tg*ISP1 and *Tg*IPS2 constructs due to the absence of tryptophan residues and by absorbance at 280 nm for *Tg*ISP3 constructs.

Crystallization and Data Collection

TgISP1—*Tg*ISP1-1 was refractory to crystallization, whereas high quality crystals of native *Tg*ISP1-2 were identified as described previously (20). *Tg*ISP1-2_SeMet was crystallized in 2.0 M ammonium sulfate, 5% isopropyl alcohol. A single *Tg*ISP1-2_SeMet crystal was looped, cryoprotected in saturated lithium sulfate, and flash-cooled at 100 K directly in the cryostream. Diffraction data were collected on beam line 08B1-1 at the Canadian Light Source at the optimized wavelength of 0.9792 Å for the *f"* selenium edge.

TgISP3—Initial crystal trials for *Tg*ISP3-1 were set in 96-well plates (Emerald Biosystems), and crystals were identified in 2.0 M sodium malonate, pH 7.0. The final sitting drops consisted of 1.5 μl of protein (14 mg/ml in HEPES-buffered saline containing 1 mM DTT) and 1.5 μl of reservoir solution and were equilibrated against 100 μl of reservoir solution. Crystals were optimized to a final condition of 2.0 M sodium malonate, pH 7.0, 10 mM betaine hydrochloride. A single *Tg*ISP3-1 crystal was looped, stepped into a final cryoprotectant of reservoir solution supplemented with 25% glycerol, and flash-cooled to 100 K directly in the cryo stream. Diffraction data were collected on beam line 11-1 at the Stanford Synchrotron Radiation Lightsource.

Data Processing, Structure Solution, and Refinement

TgISP1-2—Diffraction data for native and SeMet crystals were processed to 2.10 and 2.70 Å resolution, respectively, using Imosflm (21) and Scala (22) in the CCP4 suite of programs (23). The structure of *Tg*ISP1-2 was phased by SeMet single wavelength anomalous dispersion. A total of four selenium sites (two per monomer) were identified and refined using the SHELX C/D/E pipeline (24). High quality phases were obtained after density modification in dm (25) and enabled building and registering of ~60% of the backbone using buccaneer (26). The remaining structure was built manually and used as a molecular

TABLE 1
Data collection and refinement statistics
Values in parentheses are for the highest resolution shell. r.m.s.d., root mean square deviation; SAD, single wavelength anomalous dispersion.

	*Tg*ISP1–2 native	*Tg*ISP1–2 SeMet SAD	*Tg*ISP3–1 native
Data collection statistics			
Space group	$P2_12_12_1$	$P4_{1/3}32$	$I4_122$
a, *b*, *c* (Å)	58.11, 81.09, 120.07	128.15, 128.15, 128.15	99.48, 99.48, 60.87
α, β, γ (degree)	90, 90, 90	90, 90, 90	90, 90, 90
Wavelength (Å)	1.542	0.9792	0.9795
Resolution range (Å)	29.09-2.10 (2.21-2.10)	57.31-2.70 (2.85-2.70)	35.94-2.32 (2.41-2.32)
Measured reflections	160,946	269,737	35,300
Unique reflections	33,884	10,430	6,813
Redundancy	4.7 (4.8)	25.9 (24.0)	5.2 (4.3)
Completeness (%)	99.9 (100.0)	100.0 (100.0)	99.3 (98.9)
$I/\sigma(I)$s	16.3 (4.5)	27.2 (7.7)	18.6 (2.3)
R_{merge} [a]	0.069 (0.380)	0.088 (0.471)	0.041 (0.543)
Refinement statistics			
Resolution (Å)	28.15-2.10 (2.15-2.10)		35.94-2.32 (2.38-2.32)
R_{cryst} [b]/R_{free} [c]	0.204/0.256 (0.231/0.301)		0.218/0.268 (0.302/0.314)
No. of atoms			
Protein (A/B/C/D)	967/970/962/975		994
Solvent	273		4
Sulfate	70		N/A
B values (Å^2)			
Protein (A/B/C/D)	26.7/24.5/30.7/31.8		64.1
Solvent	31.8		46.1
Sulfate	49.3		N/A
r.m.s.d. from ideality			
Bond lengths (Å)	0.013		0.010
Bond angles (deg.)	1.28		1.15
Ramachandran statistics (%)			
Most favored	99.0		99.1
Allowed	1.0		0.9
Disallowed	0.0		0.0

[a] $R_{merge} = \sum_{hkl}\sum_i|I_{hkl,i} - [I_{hkl}]|/\sum_{hkl}\sum_i I_{hkl,i}$, where $[I_{hkl}]$ is the average of symmetry related observations of a unique reflection.
[b] $R_{cryst} = \sum|F_{obs} - F_{calc}|/\sum F_{obs}$, where F_{obs} and F_{calc} are the observed and the calculated structure factors, respectively.
[c] R_{free} is R using 5% of reflections randomly chosen and omitted from refinement.

replacement model for the higher resolution native data using Phaser (27). Solvent atoms were selected using COOT (28) and refined in Refmac5 (29). Complete structural validation was performed in Molprobity (30), and stereochemical analysis of the refined *Tg*ISP1-2 structure was performed with Rampage in CCP4 (23), with the Ramachandran plot showing excellent stereochemistry with 99% of the residues in the most favored conformations and no residues in disallowed orientations. Overall, 5% of the reflections were set aside for calculation of R_{free}. Data collection and refinement statistics are presented in Table 1.

TgISP3-1—Diffraction data for native crystals were processed to 2.32 Å resolution using the methods described for *Tg*ISP1-2. Initial phases were obtained by molecular replacement using Phaser (27) with *Tg*ISP1-2, pruned with CHAINSAW (31) to better reflect the *Tg*ISP3-1 sequence, as a search model. Refinement, structural validation, and stereochemical analysis was performed as for *Tg*ISP1-2 described above. Data collection and refinement statistics are presented in Table 1.

Accession Numbers

The atomic coordinates and structure factors have been deposited in the Protein Data Bank under the codes 4CHM (*Tg*ISP1-2) and 4CHJ (*Tg*ISP3-1).

Phospholipid Binding Assay

*Tg*ISP1-1, *Tg*ISP2-1, and *Tg*ISP3-1 were tested for their ability to bind a variety of membrane-associated lipids using Echelon Biosciences PIP Strip assay (P-6001), containing eight phosphoinositides and seven other biologically important lipids. Phosphatidylinositol 4,5-diphosphate-specific binding protein was used as a positive control, and the strips were probed according to the manufacturer's instructions.

Homology Modeling

Secondary structure predictions were performed using PsiPred to determine the core conserved elements for *Tg*ISP2 (32). A homology model for *Tg*ISP2core (Gly-40 to Ala-152) was generated using Modeler (33) embedded in Chimera (34) with chain A of *Tg*ISP1-2 as an input model. The highest confidence model (indicated by the lowest zDOPE score) was chosen and inspected manually for quality.

RESULTS

Apicomplexan ISPs Are Separated into Two Clades Represented by TgISP1 and TgISP3—In our previous study we showed that apicomplexan ISPs are broadly conserved and separated into two ortholog groups (14). Here we have performed a phylogenetic analysis on selected ISPs, showing that *Tg*ISP1, *Tg*ISP2, and *Tg*ISP4 cluster in one clade, whereas *Tg*ISP3 clusters in a distinct, second clade (Fig. 1*B*) in agreement with recent observations (16). It is noteworthy that parasites such as *T. gondii*, *Neospora caninum*, and the *Plasmodium* spp. have representatives of both the first and second ortholog groups, whereas parasites such as *Cryptosporidium* spp. have only a *Tg*ISP1/2 ortholog. Based on currently available sequence data, the tissue dwelling coccidia (*Toxoplasma*, *Neospora*, and *Eimeria* spp.) appear to be the only parasites with an ISP1 paralog (*i.e.* ISP2) (Fig. 1*B*). Although the ISPs share relatively low sequence identity, we previously found that all three *Tg*ISPs are predicted to have the same core secondary structure elements

(20), consistent with a conserved protein fold. To investigate the details of the ISP structure-function relationship, we selected *Tg*ISP1 and *Tg*ISP3 as representatives of the two apicomplexan ISP clades as well as *Tg*ISP2 to complete the panel of predominantly expressed ISPs in *T. gondii*.

Purification of the TgISPs Reveals Conformational Variability—Multiple constructs of each *Tg*ISP were produced in *E. coli* and purified by nickel-affinity and size exclusion chromatography for use in functional studies and crystallization trials. Although the three *Tg*ISP proteins are quite small, with the predicted core domain only ~120 amino acids (20), they each presented a divergence from the expected globular monomer.

Two constructs were designed for *Tg*ISP1 (Fig. 1*C*, *top*): nearly full-length (lacking the N-terminal sites for myristoylation and palmitoylation, *Tg*ISP1-1) and conserved core (*Tg*ISP1-2). *Tg*ISP1-1 (19.5 kDa) migrated during gel filtration as a single major peak corresponding to 36.4 kDa, suggesting the formation of a dimer (Fig. 1*C*, *black*). The truncated *Tg*ISP1-2 (13.9 kDa) eluted in one major peak corresponding to 16.4 kDa with two significant shoulders (Fig. 1*C*, *purple*); this elution profile suggests the presence of a conformationally impure monomer population, possibly due to redox instability given the high proportion of cysteines in this small domain (20). The gel filtration traces for both *Tg*ISP2 constructs indicate a nearly equal mixture of monomer and dimer (Fig. 1*D*), with *Tg*ISP2–2 (14.5 kDa), for example, eluting as two major peaks corresponding to molecular masses of 35.3 and 18.3 kDa (Fig. 1*D*, *blue*). The two constructs of *Tg*ISP3 showed similar elution profiles with only one major peak, likely corresponding to a semi-globular monomer (Fig. 1*E*); the major peak for *Tg*ISP3-1 (18.3 kDa) corresponds to a molecular mass of 27 kDa.

Structure Determination of TgISP1-2 and TgISP3-1—Crystallization trials were performed using all six *Tg*ISP constructs. After several rounds of optimization, diffraction quality crystals were obtained for *Tg*ISP1-2 and *Tg*ISP3-1. Consistent with the lack of sequence identity with reported structures, no suitable molecular replacement model was identified, and phases for *Tg*ISP1-2 were ultimately obtained from a SeMet single wavelength anomalous dispersion experiment. The 118-residue sequence of *Tg*ISP1-2 contains a single methionine, with the addition of a second methionine provided by the residual sequence from the tobacco etch virus protease cleavage (GSMAS). Initial heavy atom searches revealed high occupancy for four selenium sites corresponding to two molecules in the asymmetric unit (AU) of the primitive cubic unit cell. In contrast, native *Tg*ISP1-2 crystallized as a monomer with four molecules in the AU of the primitive orthorhombic unit cell (35). The four monomers of native *Tg*ISP1-2 overlay well, with root mean square deviations relative to chain A of 0.75 Å over 124 Cα (chain B), 0.95 Å over 124 Cα (chain C), and 0.79 Å over 123 Cα (chain D). All structural analyses were performed with chain A unless otherwise noted. The 2.10 Å resolution structure of *Tg*ISP1-2 is modeled completely from Ser-54 to Ala-178 (Fig. 2*A*). At both termini, the residual sequence from the expression vector was well ordered; the first *Tg*ISP1 residue modeled is Pro-58, and the last is Ala-176.

The structure of *Tg*ISP1-2 emerged as a suitable molecular replacement model for *Tg*ISP3-1, which crystallized as a monomer with one molecule in the AU of the body-centered tetragonal unit cell (35). *Tg*ISP3-1 was refined to a resolution of 2.32 Å with the final model extending from Ala-15 through Glu-153 with two regions of disorder (Fig. 2*B*). Although a significant portion of the N-terminal coil is ordered, a five-residue region between Val-25 and Ile-31 could not be modeled without ambiguity. In addition, a portion of the loop between Ser-97 and Lys-108 was disordered, although some intervening density was present.

The TgISPs Adopt a Conserved Fold—Despite sharing only 25% sequence identity, structural superposition reveals that both *Tg*ISP1 and *Tg*ISP3 adopt the same structural scaffold, as evidenced by a root mean square deviation of just 1.45 Å over 105 Cα. Overall, an N-terminal helix is positioned on the periphery of a twisted, seven-stranded antiparallel β-sandwich bordered on one end by interstrand loops (open end) and capped at the other end by an amphipathic C-terminal helix (closed end) (Fig. 2*C*). One side of the sandwich is formed by β1-β2-β3-β4, whereas the other side is formed by β5-β6-β7; for both structures this differs from the predicted secondary structure where β5 was predicted to be α-helical (20). Although the majority of connecting segments between the secondary structure elements are short turns, an extended variable loop is present between β5 and β6 (Fig. 2*C*, *dotted arrow*). In *Tg*ISP1-2, this loop contains an α-helix (Fig. 2, *A* and *C*) and along with the ordered coil packs against the core domain; in contrast, in *Tg*ISP3-1, this loop is completely coiled and extends away from the core domain, and in an unusual organization, the N-terminal coil threads through the partially disordered β5-β6 loop (Fig. 2, *B* and *C*). Additionally, a disulfide bond is present in the structure of *Tg*ISP1-2, linking the middle of β2 to the tip of β3 (Fig. 2*C*, *solid arrow*). A structure-based sequence alignment constructed from the structures of *Tg*ISP1 and *Tg*ISP3 and a high confidence homology model of *Tg*ISP2 (data not shown) support the conclusion of a conserved fold across the ISP family (Fig. 2*D*).

The ISPs Adopt a Pleckstrin Homology Fold—Having established the fold conservation of the *Tg*ISPs, we next sought to compare the ISP fold to those of known structures. A DaliLite search (36) revealed that the overall topology and organization of secondary structure elements for *Tg*ISP1-2 and *Tg*ISP3-1 (Fig. 3, *A* and *B*) displays significant similarity with PH domain-containing proteins; phospholipase Cδ1 (PLCδ1_PH; PDB ID 1MAI-A) (Fig. 3*C*) was identified as the top hit for both *Tg*ISP1-2 (Z-score of 12.4) and *Tg*ISP3-1 (Z-score of 10.8) (37). Despite showing negligible sequence identity ($\leq$15%), the clear structural homology of both *Tg*ISP1 and *Tg*ISP3 with multiple PH domains has prompted our classification of the ISP proteins as adopting a PH fold. It is noteworthy that low sequence identity is commonly observed between characterized PH domains and explains why this domain was not readily apparent in earlier bioinformatic analyses. The N-terminal helix of both *Tg*ISP1-2 and *Tg*ISP3-1 (Fig. 3) is not part of the canonical PH domain; however, a short helix in this position is observed in some other PH domain-containing proteins such as PLCδ1 (37).

PH domains typically mediate protein-lipid and protein-protein interactions in diverse protein families. Their function is

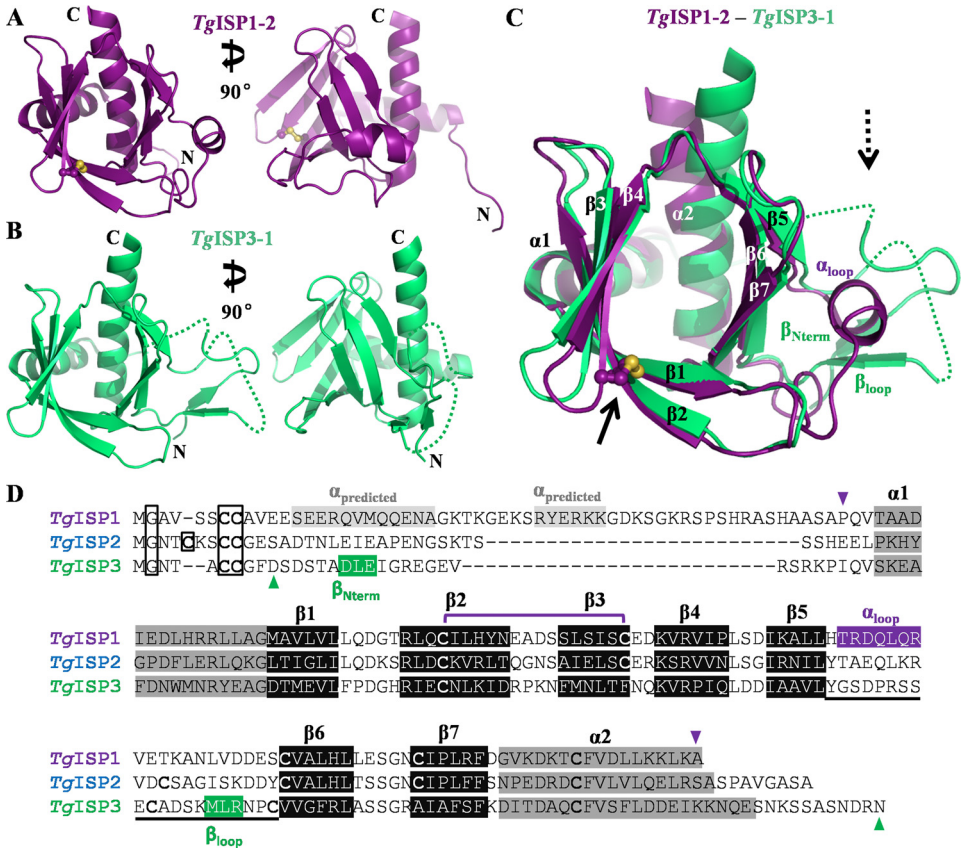

FIGURE 2. **Structural characterization of *Tg*ISP1-2 and *Tg*ISP3-1 reveals conservation of a similar fold across both apicomplexan ISP phylogenetic clades.** *A*, orthogonal views of *Tg*ISP1-2 shown as a purple schematic with the disulfide bond shown in ball-and-stick representation. *B*, orthogonal views of *Tg*ISP3-1 shown as a *green schematic*; *dotted lines* indicate connectivity of disordered loops. *C*, overlay of *Tg*ISP1-2 (*purple schematic*) on *Tg*ISP3-1 (*green schematic*). Although the core fold is clearly conserved, *arrows* indicate the two major regions of divergence between the two proteins. *Solid arrow*, β2-β3 disulfide bond of *Tg*ISP1-2. *Dashed arrow*, β5-β6 loop and N-term positioning. *D*, structure-based sequence alignment of *Tg*ISP1, *Tg*ISP2 (based on homology model), and *Tg*ISP3. *Triangles* indicate the crystallized constructs; *boxed Gly/Cys residues* are lipidated; the divergent β5-β6 loop is *underlined*.

best characterized in higher eukaryote proteins with little known about the role of proteins containing this fold in single celled organisms. In fact, PH-like domains were only recently identified in bacteria (38). The structures of *Tg*ISP1-2 and *Tg*ISP3-1 presented here are, to our knowledge, the first structural characterization of PH domains from a eukaryotic pathogen.

TgISP PH Domains Are Cysteine-rich with a Unique Disulfide in the ISP1 Ortholog Group—All three of the major *Tg*ISP proteins have notably high cysteine content in the core domain. The 176-residue *Tg*ISP1 contains 7 cysteines (5 in the core domain), and the 160-residue *Tg*ISP2 contains 9 cysteines (6 in the core domain), whereas *Tg*ISP3 is 164 residues and contains 6 cysteines (4 in the core domain). Despite being intracellular proteins, the structure of *Tg*ISP1-2 shows one disulfide bond linking the middle of β2 to the tip of β3 (Cys-90 to Cys-105; Fig. 3*A*, *black arrow*), which generates a more compact core domain. Of the three free cysteines, two (Cys-142 and Cys-166) are somewhat buried, whereas one (Cys-153) is surface-exposed and displays two conformations (Fig. 3*A*). A disulfide bond between β2 and β3 is likely a structural feature of the *Tg*ISP1 ortholog group, as both cysteines appear broadly conserved, with the exception of *Tg*ISP1 orthologs in *Cryptosporidium* (14). A disulfide is also predicted in a similar position for *Tg*ISP2 (Fig. 2*D*). *Tg*ISP3 does not cluster with the *Tg*ISP1 ortholog group (14) (Fig. 1*A*). Cys-105 of *Tg*ISP1 is not conserved in *Tg*ISP3 (Fig. 2*D*), and no disulfide bonds are present in the structure of *Tg*ISP3-1 (Fig. 3*B*). However, Cys-114 at the base of β6 is surface-exposed and capped with a β-mercaptoethanol molecule (Fig. 3*B*). In addition, Cys-104 is not modeled but would be surface-exposed and part of the extended β5-β6 loop. The cysteine-rich nature of the *Tg*ISPs and the number of surface-exposed cysteines may result in redox instability and explain the multiple conformations observed during purification (Fig. 1*C*) (20) and may also facilitate higher order multimerization (Fig. 1*D*).

Of the numerous structurally characterized PH domains, a high cysteine content is relatively uncommon but is present in selected PH domains such as Evectin-2 PH (PDB ID 3VIA). Furthermore, only two disulfide bond positions have been reported in characterized PH domains. The PH domain of DAPP1/PHISH (for example PDB ID 1FB8) has a disulfide linking the base of β6 to the tip of β7, whereas the PH domains of PKBα/PKBβ/AKT1 (for example PDB IDs 1UNP/1P6S/3O96) have a disulfide linking the base of β5 to the tip of β6. Therefore, the disulfide found in *Tg*ISP1-2 (Fig. 3*A*) is unique among structurally characterized PH domains. It is worth noting that the structure of the kindlin-2 PH domain (PDB ID 4F7H) shows two free cysteines in the same backbone positions as the disul-

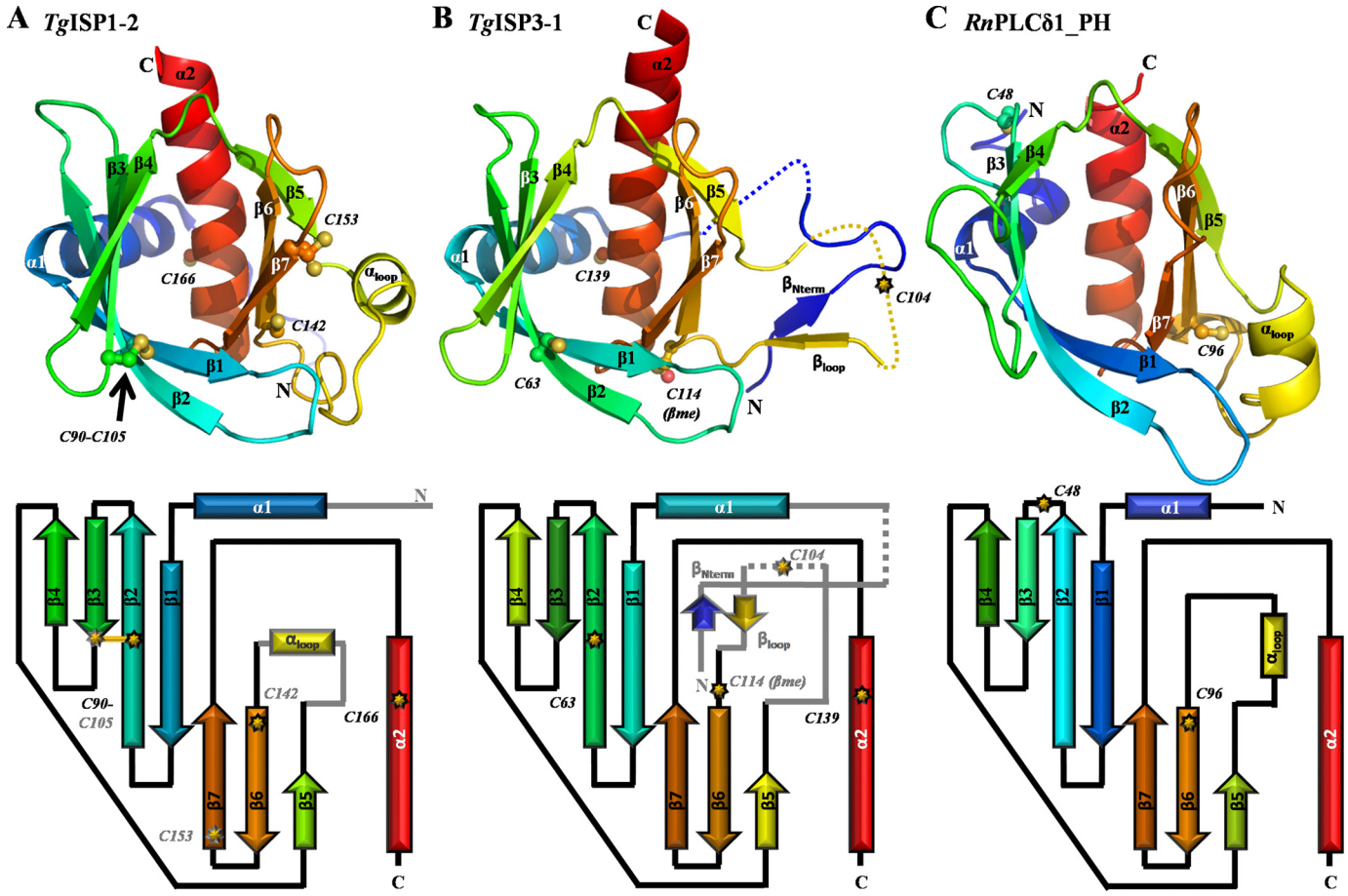

FIGURE 3. **The ISPs adopt a pleckstrin homology fold.** *A*, *top*, secondary structure depiction of *Tg*ISP1-2 colored in rainbow from N (*blue*) to C (*red*). Note: the extended ordering of the N terminus in *Tg*ISP3 leads to a shift in the rainbow throughout the secondary structure elements. The *black arrow* indicates the single disulfide bond. *Bottom*, topology diagram for the PH fold of *Tg*ISP1-2; common features with *Tg*ISP3-1 are shown as *black outlined arrows* (β-strands) and *rectangles* (α-helices) with *black connectors*. Features specific to *Tg*ISP1-2 are shown in gray. *B*, *top*, secondary structure depiction of *Tg*ISP3-1 colored as in *A*. *Dotted lines* indicate the two unmodeled loops in the crystal structure. *Bottom*, topology diagram as described in *A*. *C*, *top*, secondary structure depiction of phospholipase C-δ 1 (PDB ID 1MAI-A). *Bottom*, topology diagram.

fide bound cysteines of *Tg*ISP1-2; however, the side chains are directed away from the disulfide axis.

The Phospholipid Binding Properties of Many PH Domains Are Not Conserved in the TgISPs—The vast majority of proteins containing a PH domain are multimodular, with some PH domains having a membrane anchoring role through an interaction with inositol phosphate (IP) head groups of membrane-associated phosphatidylinositides (39, 40). In fact, the PH domain of PLCδ1, which displays the highest structural similarity to the PH domain of *Tg*ISP1-2 and *Tg*ISP3-1, binds inositol-1,4,5-trisphosphate with high affinity (37). We, therefore, tested the ability of the recombinant *Tg*ISPs to coordinate a variety of mono-, di-, and tri-phosphorylated phosphatidylinositols and seven other biologically relevant lipids including phosphatidylserine using commercial lipid arrays. Despite obtaining expected results with the positive control protein, no detectable interaction was observed between the nearly full-length constructs of *Tg*ISP1, *Tg*ISP2, or *Tg*ISP3 with any of the tested phospholipids (data not shown).

DISCUSSION

The ISPs are small single domain proteins conserved across phylum Apicomplexa (Fig. 1*B*) that are critical for proper asexual cell division in *T. gondii* (14) and for defining apical polarity in *P. berghei* (16). Our structural and biochemical characterization of the three major *Tg*ISPs revealed unexpected and intriguing layers of complexity imparted by conformational heterogeneity, multimerization, and semi-globular forms (Fig. 1) assembled around a PH core.

Comparative Structural Analysis Supports the Absence of TgISP Phospholipid Binding Properties—Classically, PH domains play important roles in mediating membrane localization through IP binding (41). Key structural features that mediate these interactions are apparent. For example, a highly basic patch on the surface of PLCδ1_PH is readily observed as the binding pocket for the phospholipid headgroup (Fig. 4*A*, *top*), with numerous specific interactions between a cluster of basic residues and the phosphates (Fig. 4*A*, *bottom*). A consensus motif for binding 3-phosphoinositide was previously proposed, with numerous basic residues located in β1, the β1-β2 loop, β2, β4, and β7, and Tyr in β3 governing specificity (40, 42). The general importance of this basic patch is also observed in the PH domain of Evectin-2, which mediates phosphatidylserine, but not IP, binding (43). Although basic residues are observed in the *Tg*ISPs on the same face of the molecule, the number of residues

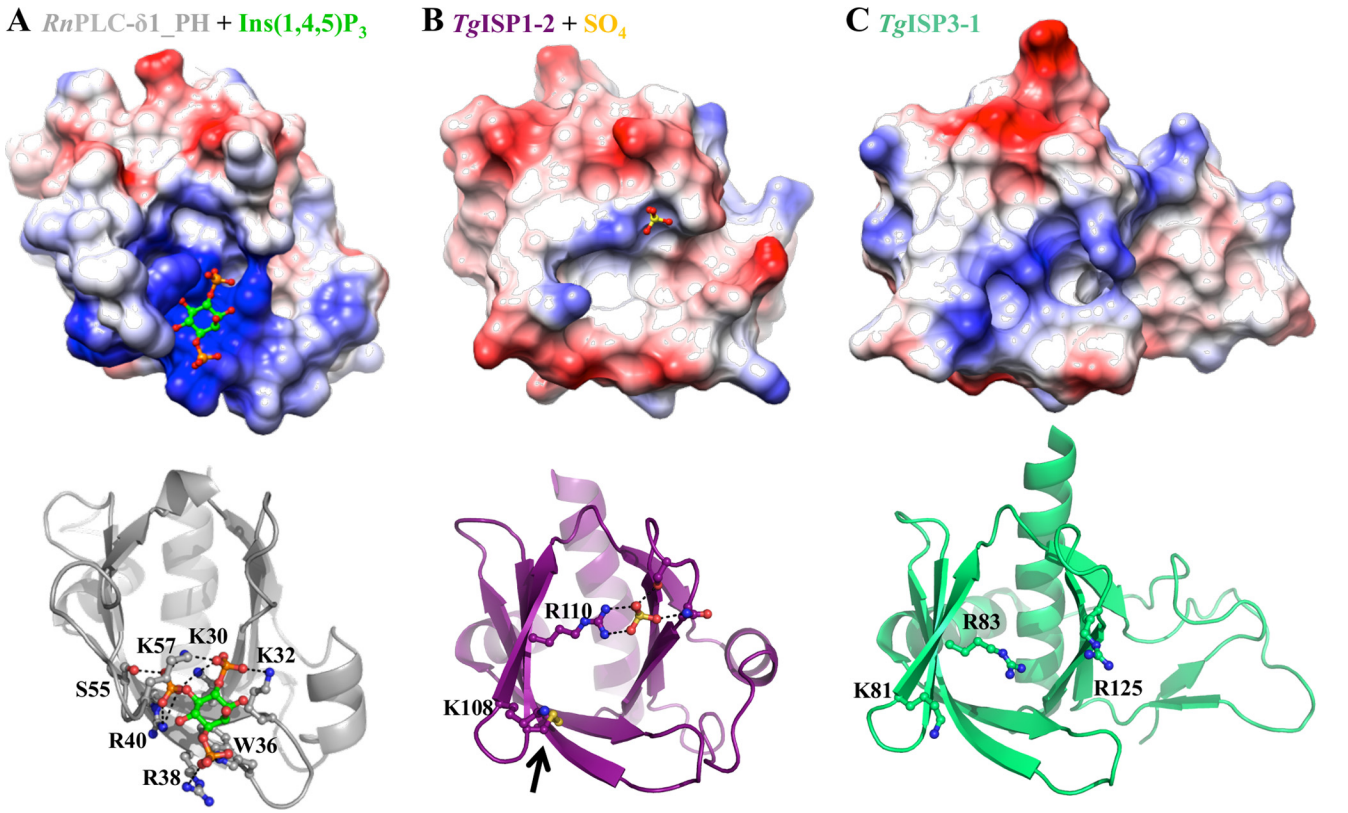

FIGURE 4. **Surface analysis and basic side chain distribution support the lack of a phospholipid binding role for the *Tg*ISPs.** *A*, chimera (34) coulombic-colored surface representation of the PH domain of phospholipase Cδ1 (PLCδ1_PH; PDB ID 1MAI) shows a concentration of basic charge around the inositol-(1,4,5)-trisphosphate (*Ins(1,4,5)P3*, *green ball-and-stick* representation) binding site at the bottom of the molecule open end (*top*), which is due to a clustering of basic residues forming specific interactions with the ligand (*bottom*). *B*, *Tg*ISP1-2; coulombic-colored surface shows a strong hydrophobic patch and just two basic residues forming separate small basic patches (*top*); a sulfate ion is seen coordinated predominately by Arg-110 near the top of the open end, and the constraining disulfide bond is indicated by a *black arrow* (*bottom*). *C*, *Tg*ISP3-1; coulombic-colored surface shows both basic and hydrophobic character (*top*), but the residues are dispersed (*bottom*).

and their organization strongly support the biochemically observed lack of phospholipid headgroup binding. For *Tg*ISP1, Lys-108 and Arg-110 are the only positively charged residues in the region, and the high sulfate concentrations used during crystallization resulted in a single sulfate bound to Arg-110 in a position that is inconsistent with any of the phosphates of the IP bound to PLCδ1_PH (Fig. 4*B*). In fact, the disulfide bond of *Tg*ISP1-2 (and likely other ISP1 orthologs) lies within the region of IP coordination of other PH domains and restricts rearrangement of the β3-β4 loop that would likely be required for spatial accommodation of a phospholipid headgroup (Fig. 4*B*, *bottom*). For *Tg*ISP3, Lys-81 and Arg-83 are analogous to the Lys/Arg pair in *Tg*ISP1. *Tg*ISP3 additionally contains Arg-125 on β7, but a clustering of the residues was not observed (Fig. 4*C*). Thus the divergent surface chemistry of the *Tg*ISPs relative to classical PH domains correlates with the lack of observed phospholipid binding. It is not necessarily surprising that *Tg*ISPs do not require phospholipid binding functionality given that they each harbor multiple N-terminal residues predicted to be myristoylated or palmitoylated (Fig. 2*D*), leading to proper localization and anchoring to the IMC. Indeed, membrane anchorage by these acylated N-terminal residues may position the key IP interacting face of each ISP PH domain away from the membrane surface (see Fig. 6).

Structural Analysis of the ISPs in the Context of PH Domain Interactions Suggests a Protein Binding Functional Mechanism—The majority of PH-phospholipid interactions characterized thus far show coordination of the IP or phosphatidylserine by the inner face of the β1-β2-β3-β4 sheet, with atypical coordination by the outer face of the β1-β2 and β5-β6 loops (Fig. 5*A*, *left*). However, an increasing number of studies imply a much broader functional range for PH domains with mounting evidence supporting roles in protein-protein interactions that employ several surfaces on the PH scaffold (Fig. 5*A*, *right*) (44, 45). For example, PH domains have been found to use a number of basic residues located on β1 and β2 to bind filamentous actin (46), a cleft between β5 and the C-terminal helix to accommodate phosphotyrosine peptides (47), or the outer surface of the β5-β6-β7 sheet to bind polyproline peptides (48). In fact, nearly every possible surface on the PH domain scaffold has been shown to bind a protein partner or facilitate interdomain interactions of multimodular proteins (44). From these analyses it is clear that PH domains have a high degree of plasticity supported by the ability to functionalize different regions of the PH fold.

Based on the current knowledge of PH domain functions combined with the lack of any observable affinity of the *Tg*ISPs for IPs, we hypothesize that the *Tg*ISPs have protein binding partners. Because the *Tg*ISPs were shown to be tightly regulated

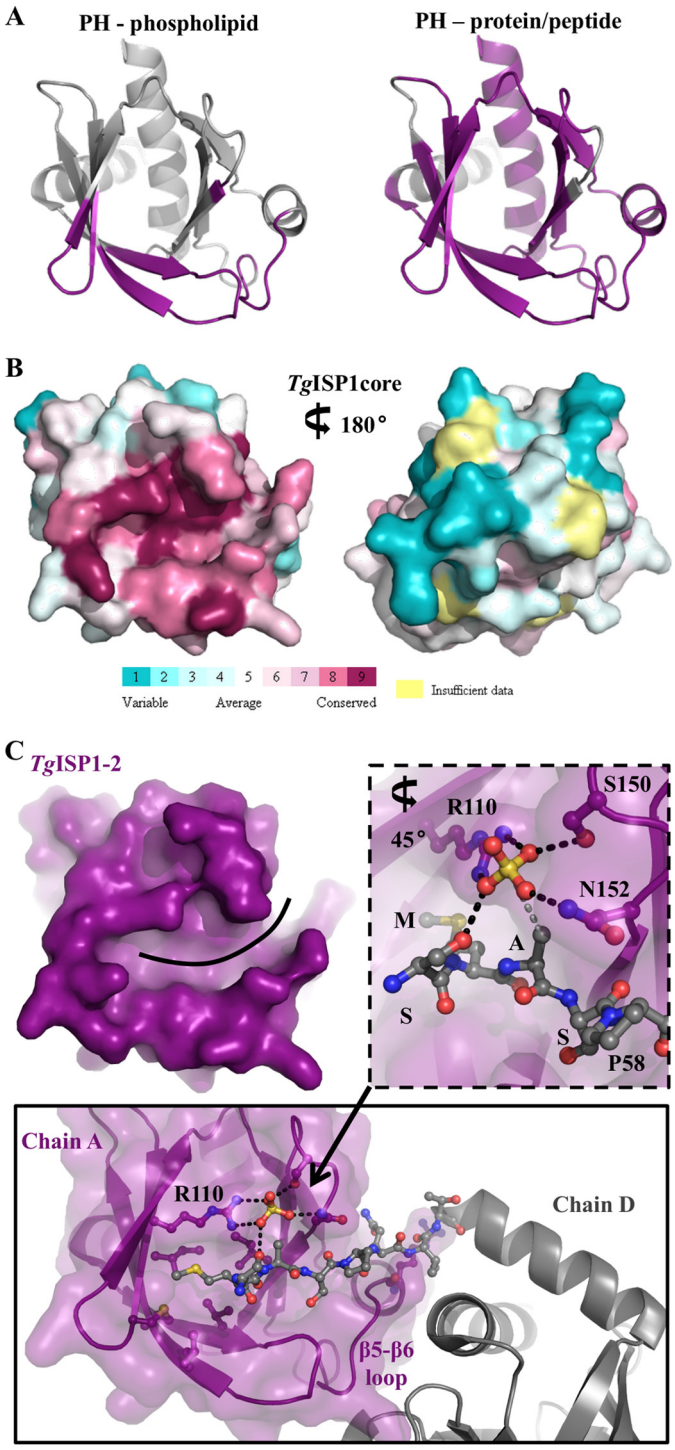

FIGURE 5. **The region corresponding to lipid binding functionality observed for other PH domains is highly conserved in the apicomplexan ISPs and capable of coordinating a polypeptide structure in *Tg*ISP1.** *A*, surfaces on PH domains identified to mediate interactions with phospholipid headgroups (*left*) or proteins/peptides (*right*) are mapped in *purple* onto *Tg*ISP1. *B*, mapping of conserved (*burgundy*) and variable (*teal*) residues onto the *Tg*ISP1core using ConSurf (19) shows a clear bias for conservation on one side of the protein. Viewpoint in (*B*, *left*) is aligned with *Rn*PLC-δ1 of Fig. 4*A*. *C*, *left*, the *purple surface* of *Tg*ISP1-2 shows a deep groove (*black line*) that partially overlays with the phospholipid binding region of other PH domains. *Bottom*, in every chain of the AU in two different space groups, the N terminus of a neighboring chain (*gray schematic*; SMASPQV sequence is shown as in *ball and stick representation*) buries into the surface groove. *Inset*, the positioning of the sulfate ion coordinated by the highly conserved Arg-110 is consistent with an acidic or phosphorylated amino acid at the *A* position (*gray dotted line*).

during cell division with highly specific localization patterns (14), a protein-protein interaction functional mechanism would fit with the *Tg*ISPs recruiting protein partners to specific sub-compartments of the IMC to enable proper daughter cell formation. Although our initial attempts to identify a binding partner for *Tg*ISP1 were unsuccessful (14), the possibility of interactions that are lower affinity, transient, or specific to a certain stage in the cell cycle remains a possibility.

Conservation Analysis Suggests the TgISPs Repurpose the Phospholipid-binding Site—To hone in on which surface of the PH scaffold is most likely to be utilized by the ISPs, an analysis of the distribution of conserved and variable residues across all known apicomplexan ISP sequences was mapped onto the *Tg*ISP1core structure using the ConSurf server (19). Conservation mapping showed a clear bias of conserved residues on the open side of the molecule composed of the β1-β2, β3-β4, and β6-β7 loops (Fig. 5*B*); this surface overlaps significantly with the phospholipid binding pocket of other PH domains. Given the highly polarized distribution of conserved residues, the ISPs likely maintain a conserved function utilizing the surface at the open end of the PH domain.

Crystal Packing Suggests a Possible Mechanism for TgISP Protein Binding Functionality—An indication of how the ISPs might coordinate a protein partner in this area can be observed in the deep groove present on the surface of *Tg*ISP1-2 (Fig. 5*C*, *left*), and the ability of this groove to coordinate the N-terminal tail of a neighboring molecule (Fig. 5*C*, *bottom*). Although this specific coordination event may be an artifact of crystallization, it is interesting that it is observed in both the *Tg*ISP1-2 cubic and orthorhombic crystal forms. Ultimately, the observed association does offer insight into a possible mechanism of macromolecular assembly. Overall, nearly 2200 Å^2 of surface area is buried at the interface between the two chains, with β7 and the β5-β6 loop of one molecule forming 14 hydrogen bonds with the N-terminal tail, β5-β6 loop, and C-terminal helix of a neighboring molecule (35). More than 50% of the total buried surface at the interface of the two molecules is due to the extended, buried N-terminal residues. In particular, a Met residue buries into a deep pocket lined by hydrophobic residues (Fig. 5*C*, *bottom*). Although the individual residues are not conserved with *Tg*ISP3, a similar hydrophobic pocket is present. Additionally, *Tg*ISP1 Arg-110, which is completely conserved among known apicomplexan ISP sequences (Fig. 5*B*), coordinates a sulfate ion that sits 4 Å from the N-terminal Ala residue (Fig. 5*C*, *inset*). It is tempting to speculate that the binding site on the physiological partner for each ISP has a strong hydrophobic component adjacent to a negatively charged or phosphorylated amino acid. Ultimately, the presence of the groove on *Tg*ISP1 that can accommodate a non-native peptide may highlight the fundamental plasticity of this region to promote complex formation between divergent partners.

Multimerization and Phosphorylation May Play a Role in Regulating Biologically Relevant Forms of TgISPs—Multimerization may also contribute to the specific functions of each of the *Tg*ISPs, possibly by providing composite interaction surfaces or increasing the avidity of ligand binding (Fig. 6) (49). Based on reproducible size exclusion chromatograms, *Tg*ISP1 dimerization appears to be dependent on the presence of the

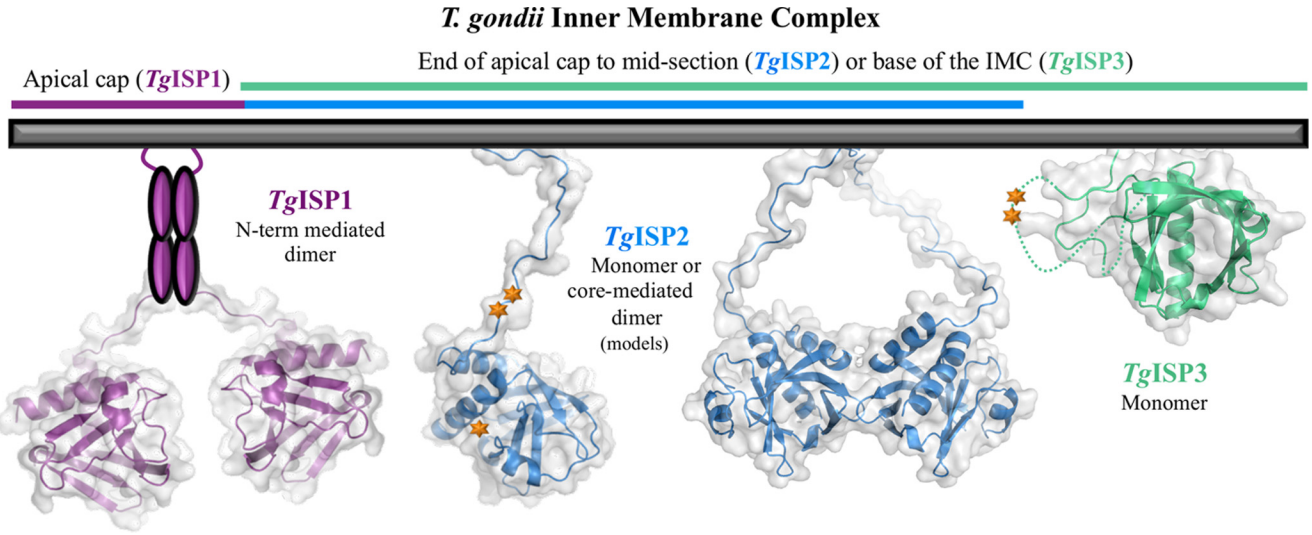

FIGURE 6. **Multimeric state may play a role in ISP function.** A schematic representation of experimentally supported organizations of the ISPs on the inner membrane complex of *T. gondii* is shown. ISP structures and homology models are shown as a colored schematic backbone with a *semi-transparent gray surface*. *Purple ovals* represent predicted N-terminal helices of *Tg*ISP1. *Orange starbursts* indicate phosphorylation sites. *Tg*ISP1 core and *Tg*ISP3 full were structurally determined, whereas *Tg*ISP2 full-length monomer and dimer are homology models.

full N-terminal tail (Figs. 1*C* and 6), which is predicted to contain ordered regions of secondary structure (Fig. 2*D*). The native N-terminal tails of *Tg*ISP1 are unlikely to promote dimerization through interactions with the surface groove as no strongly hydrophobic residues are present in the coil regions with the structural flexibility to be coordinated in the groove (Fig. 2*D*); also, this type of N-terminal interaction with the core domain of a second molecule generates an oligomer in the crystal, not a distinct dimer as observed in gel filtration. *Tg*ISP2 has a long N-terminal tail predicted to be disordered (Fig. 2*D*), and the elements mediating the monomer-dimer equilibrium are fully retained in the core domain (Figs. 1*D* and 6). Finally, the way that the *Tg*ISP3 N-terminal tail wraps loosely around the core domain and through the $\beta5$-$\beta6$ loop helps explain its semi-globular nature (Figs. 1*E* and 6), and the monomeric state of *Tg*ISP3 is consistent with the crystal structure; only one molecule in the AU that does not show significant interaction interfaces with any neighboring molecules.

Phosphorylation may also play a role in ISP function, either influencing the ability to dimerize or to interact with other binding partners. A previous study on the phosphoproteomes of *T. gondii* and *Plasmodium falciparum* revealed that *Pf*ISP3, *Tg*ISP2, and *Tg*ISP3 are all phosphorylated in the parasites (50). Based on our structures and homology model, the three phosphorylation sites on *Tg*ISP2 map to a tandem pair of serine residues in the N-terminal tail and a serine at the tip of the $\beta2$-$\beta3$ loop, whereas the two sites on *Tg*ISP3 map to a tandem pair of serines in the $\beta5$-$\beta6$ loop that is disordered in the structure (Fig. 6). A more recent study showed evidence for phosphorylation of both *P. berghei* ISP1 and *Pb*ISP3, with a parasite life-cycle stage-specific pattern of modification (16). The presence of phosphorylation sites combined with the potential for multimerization reveals an intriguingly complex repertoire of ISP forms that may help to fine-tune their critical biological functions.

Conclusions—The ISP family of proteins is present throughout phylum Apicomplexa and has been shown in *T. gondii* to be critical for proper daughter cell formation. Here we present the first structures from the ISP family (*Tg*ISP1 and *Tg*ISP3) representing both ISP phylogenetic clades and show that they adopt a pleckstrin homology fold. A number of PH domains contain high affinity binding sites for membrane-associated inositol phosphates, but this functionality is not retained in the ISPs. Given more recent evidence for the involvement of PH domains in protein-protein interactions and the presence of a conserved region that in *Tg*ISP1-2 has the ability to coordinate an extended polypeptide structure, we postulate that the ISPs facilitate proper cell division by recruiting critical proteins to the appropriate sub-compartment of the inner membrane complex.

Acknowledgment—We gratefully acknowledge the staff at Stanford Synchrotron Radiation Lightsource and Canadian Light Source.

REFERENCES

1. World Health Organization. (2010) *World Malaria Report*, World Health Organization, Geneva, Switzerland
2. Hill, D. E., Chirukandoth, S., and Dubey, J. P. (2005) Biology and epidemiology of *Toxoplasma gondii* in man and animals. *Anim. Health Res. Rev.* **6,** 41–61
3. Porchet, E., and Torpier, G. (1977) [Freeze fracture study of *Toxoplasma* and *Sarcocystis* infective stages (author's transl.). *Z. Parasitenkd.* **54,** 101–124
4. D'Haese, J., Mehlhorn, H., and Peters, W. (1977) Comparative electron microscope study of pellicular structures in coccidia (*Sarcocystis*, *Besnoitia*, and *Eimeria*). *Int. J. Parasitol.* **7,** 505–518
5. Mann, T., and Beckers, C. (2001) Characterization of the subpellicular network, a filamentous membrane skeletal component in the parasite *Toxoplasma gondii*. *Mol. Biochem. Parasitol* **115,** 257–268
6. Morrissette, N. S., Murray, J. M., and Roos, D. S. (1997) Subpellicular microtubules associate with an intramembranous particle lattice in the protozoan parasite *Toxoplasma gondii*. *J. Cell Sci.* **110,** 35–42
7. Keeley, A., and Soldati, D. (2004) The glideosome: a molecular machine powering motility and host-cell invasion by Apicomplexa. *Trends Cell Biol.* **14,** 528–532
8. Striepen, B., Jordan, C. N., Reiff, S., and van Dooren, G. G. (2007) Building

the perfect parasite: cell division in *Apicomplexa*. *PLoS Pathog.* **3,** e78
9. Gaskins, E., Gilk, S., DeVore, N., Mann, T., Ward, G., and Beckers, C. (2004) Identification of the membrane receptor of a class XIV myosin in *Toxoplasma gondii*. *J. Cell Biol.* **165,** 383–393
10. Bullen, H. E., Tonkin, C. J., O'Donnell, R. A., Tham, W. H., Papenfuss, A. T., Gould, S., Cowman, A. F., Crabb, B. S., and Gilson, P. R. (2009) A novel family of apicomplexan glideosome-associated proteins with an inner membrane-anchoring role. *J. Biol. Chem.* **284,** 25353–25363
11. Rayavara, K., Rajapandi, T., Wollenberg, K., Kabat, J., Fischer, E. R., and Desai, S. A. (2009) A complex of three related membrane proteins is conserved on malarial merozoites. *Mol. Biochem. Parasitol* **167,** 135–143
12. de Miguel, N., Lebrun, M., Heaslip, A., Hu, K., Beckers, C. J., Matrajt, M., Dubremetz, J. F., and Angel, S. O. (2008) *Toxoplasma gondii* Hsp20 is a stripe-arranged chaperone-like protein associated with the outer leaflet of the inner membrane complex. *Biol. Cell* **100,** 479–489
13. Chaudhary, K., Donald, R. G., Nishi, M., Carter, D., Ullman, B., and Roos, D. S. (2005) Differential localization of alternatively spliced hypoxanthine-xanthine-guanine phosphoribosyltransferase isoforms in *Toxoplasma gondii*. *J. Biol. Chem.* **280,** 22053–22059
14. Beck, J. R., Rodriguez-Fernandez, I. A., de Leon, J. C., Huynh, M. H., Carruthers, V. B., Morrissette, N. S., and Bradley, P. J. (2010) A novel family of *Toxoplasma* IMC proteins displays a hierarchical organization and functions in coordinating parasite division. *PLoS Pathog.* **6,** e1001094
15. Fung, C., Beck, J. R., Robertson, S. D., Gubbels, M. J., and Bradley, P. J. (2012) *Toxoplasma* ISP4 is a central IMC sub-compartment protein whose localization depends on palmitoylation but not myristoylation. *Mol. Biochem. Parasitol* **184,** 99–108
16. Poulin, B., Patzewitz, E. M., Brady, D., Silvie, O., Wright, M. H., Ferguson, D. J., Wall, R. J., Whipple, S., Guttery, D. S., Tate, E. W., Wickstead, B., Holder, A. A., and Tewari, R. (2013) Unique apicomplexan IMC sub-compartment proteins are early markers for apical polarity in the malaria parasite. *Biol. Open* **2,** 1160–1170
17. Edgar, R. C. (2004) MUSCLE: multiple sequence alignment with high accuracy and high throughput. *Nucleic Acids Res.* **32,** 1792–1797
18. Tamura, K., Peterson, D., Peterson, N., Stecher, G., Nei, M., and Kumar, S. (2011) MEGA5: molecular evolutionary genetics analysis using maximum likelihood, evolutionary distance, and maximum parsimony methods. *Mol. Biol. Evol.* **28,** 2731–2739
19. Ashkenazy, H., Erez, E., Martz, E., Pupko, T., and Ben-Tal, N. (2010) ConSurf 2010: calculating evolutionary conservation in sequence and structure of proteins and nucleic acids. *Nucleic Acids Res.* **38,** W529–W533
20. Tonkin, M. L., Brown, S., Beck, J. R., Bradley, P. J., and Boulanger, M. J. (2012) Purification, crystallization and preliminary X-ray diffraction analysis of inner membrane complex (IMC) sub-compartment protein 1 (ISP1) from *Toxoplasma gondii*. *Acta Crystallogr Sect. F. Struct. Biol. Cryst. Commun* **68,** 832–834
21. Battye, T. G., Kontogiannis, L., Johnson, O., Powell, H. R., and Leslie, A. G. (2011) iMOSFLM: a new graphical interface for diffraction-image processing with MOSFLM. *Acta Crystallogr. D Biol. Crystallogr.* **67,** 271–281
22. Evans, P. (2006) Scaling and assessment of data quality. *Acta Crystallogr. D Biol. Crystallogr.* **62,** 72–82
23. Winn, M. D., Ballard, C. C., Cowtan, K. D., Dodson, E. J., Emsley, P., Evans, P. R., Keegan, R. M., Krissinel, E. B., Leslie, A. G., McCoy, A., McNicholas, S. J., Murshudov, G. N., Pannu, N. S., Potterton, E. A., Powell, H. R., Read, R. J., Vagin, A., and Wilson, K. S. (2011) Overview of the CCP4 suite and current developments. *Acta Crystallogr. D Biol. Crystallogr.* **67,** 235–242
24. Sheldrick, G. M. (2010) Experimental phasing with SHELXC/D/E: combining chain tracing with density modification. *Acta Crystallogr. D. Biol. Crystallogr.* **66,** 479–485
25. Cowtan, K. (1994) dm: an automated procedure for phase improvement by density modification. *Joint CCP4 and ESF-EACBM Newsletter on Protein Crystallography* **31,** 34–38
26. Cowtan, K. (2008) Fitting molecular fragments into electron density. *Acta Crystallogr. D. Biol. Crystallogr.* **64,** 83–89
27. McCoy, A. J. (2007) Solving structures of protein complexes by molecular replacement with Phaser. *Acta Crystallogr. D. Biol. Crystallogr.* **63,** 32–41
28. Emsley, P., and Cowtan, K. (2004) Coot: model-building tools for molecular graphics. *Acta Crystallogr. D. Biol. Crystallogr.* **60,** 2126–2132
29. Murshudov, G. N., Vagin, A. A., and Dodson, E. J. (1997) Refinement of macromolecular structures by the maximum-likelihood method. *Acta Crystallogr. D. Biol. Crystallogr.* **53,** 240–255
30. Chen, V. B., Arendall, W. B., 3rd, Headd, J. J., Keedy, D. A., Immormino, R. M., Kapral, G. J., Murray, L. W., Richardson, J. S., and Richardson, D. C. (2010) MolProbity: all-atom structure validation for macromolecular crystallography. *Acta Crystallogr. D. Biol. Crystallogr.* **66,** 12–21
31. Schwarzenbacher, R., Godzik, A., Grzechnik, S. K., and Jaroszewski, L. (2004) The importance of alignment accuracy for molecular replacement. *Acta Crystallogr. D. Biol. Crystallogr.* **60,** 1229–1236
32. McGuffin, L. J., Bryson, K., and Jones, D. T. (2000) The PSIPRED protein structure prediction server. *Bioinformatics* **16,** 404–405
33. Eswar, N., Webb, B., Marti-Renom, M. A., Madhusudhan, M. S., Eramian, D., Shen, M. Y., Pieper, U., and Sali, A. (2006) Comparative protein structure modeling using Modeller. *Curr. Protoc. Bioinformatics*, Chapter 5, Unit 5.6, doi: 10.1002/0471250953.bi0506s15
34. Pettersen, E. F., Goddard, T. D., Huang, C. C., Couch, G. S., Greenblatt, D. M., Meng, E. C., and Ferrin, T. E. (2004) UCSF Chimera: a visualization system for exploratory research and analysis. *J. Comput Chem.* **25,** 1605–1612
35. Krissinel, E., and Henrick, K. (2007) Inference of macromolecular assemblies from crystalline state. *J. Mol. Biol.* **372,** 774–797
36. Holm, L., and Park, J. (2000) DaliLite workbench for protein structure comparison. *Bioinformatics* **16,** 566–567
37. Ferguson, K. M., Lemmon, M. A., Schlessinger, J., and Sigler, P. B. (1995) Structure of the high affinity complex of inositol trisphosphate with a phospholipase C pleckstrin homology domain. *Cell* **83,** 1037–1046
38. Xu, Q., Bateman, A., Finn, R. D., Abdubek, P., Astakhova, T., Axelrod, H. L., Bakolitsa, C., Carlton, D., Chen, C., Chiu, H. J., Chiu, M., Clayton, T., Das, D., Deller, M. C., Duan, L., Ellrott, K., Ernst, D., Farr, C. L., Feuerhelm, J., Grant, J. C., Grzechnik, A., Han, G. W., Jaroszewski, L., Jin, K. K., Klock, H. E., Knuth, M. W., Kozbial, P., Krishna, S. S., Kumar, A., Marciano, D., McMullan, D., Miller, M. D., Morse, A. T., Nigoghossian, E., Nopakun, A., Okach, L., Puckett, C., Reyes, R., Rife, C. L., Sefcovic, N., Tien, H. J., Trame, C. B., van den Bedem, H., Weekes, D., Wooten, T., Hodgson, K. O., Wooley, J., Elsliger, M. A., Deacon, A. M., Godzik, A., Lesley, S. A., and Wilson, I. A. (2010) Bacterial pleckstrin homology domains: a prokaryotic origin for the PH domain. *J. Mol. Biol.* **396,** 31–46
39. Kavran, J. M., Klein, D. E., Lee, A., Falasca, M., Isakoff, S. J., Skolnik, E. Y., and Lemmon, M. A. (1998) Specificity and promiscuity in phosphoinositide binding by pleckstrin homology domains. *J. Biol. Chem.* **273,** 30497–30508
40. Ferguson, K. M., Kavran, J. M., Sankaran, V. G., Fournier, E., Isakoff, S. J., Skolnik, E. Y., and Lemmon, M. A. (2000) Structural basis for discrimination of 3-phosphoinositides by pleckstrin homology domains. *Mol. Cell* **6,** 373–384
41. Lemmon, M. A. (2007) Pleckstrin homology (PH) domains and phosphoinositides. *Biochem. Soc. Symp.* **74,** 81–93
42. Isakoff, S. J., Cardozo, T., Andreev, J., Li, Z., Ferguson, K. M., Abagyan, R., Lemmon, M. A., Aronheim, A., and Skolnik, E. Y. (1998) Identification and analysis of PH domain-containing targets of phosphatidylinositol 3-kinase using a novel in vivo assay in yeast. *EMBO J.* **17,** 5374–5387
43. Uchida, Y., Hasegawa, J., Chinnapen, D., Inoue, T., Okazaki, S., Kato, R., Wakatsuki, S., Misaki, R., Koike, M., Uchiyama, Y., Iemura, S., Natsume, T., Kuwahara, R., Nakagawa, T., Nishikawa, K., Mukai, K., Miyoshi, E., Taniguchi, N., Sheff, D., Lencer, W. I., Taguchi, T., and Arai, H. (2011) Intracellular phosphatidylserine is essential for retrograde membrane traffic through endosomes. *Proc. Natl. Acad. Sci. U.S.A.* **108,** 15846–15851
44. Scheffzek, K., and Welti, S. (2012) Pleckstrin homology (PH) like domains: versatile modules in protein-protein interaction platforms. *FEBS Lett.* **586,** 2662–2673
45. Lemmon, M. A. (2004) Pleckstrin homology domains: not just for phosphoinositides. *Biochem. Soc. Trans.* **32,** 707–711
46. Yao, L., Janmey, P., Frigeri, L. G., Han, W., Fujita, J., Kawakami, Y., Apgar, J. R., and Kawakami, T. (1999) Pleckstrin homology domains interact with filamentous actin. *J. Biol. Chem.* **274,** 19752–19761
47. Zhou, M. M., Huang, B., Olejniczak, E. T., Meadows, R. P., Shuker, S. B.,

Miyazaki, M., Trüb, T., Shoelson, S. E., and Fesik, S. W. (1996) Structural basis for IL-4 receptor phosphopeptide recognition by the IRS-1 PTB domain. *Nat. Struct. Biol.* **3,** 388–393

48. Prehoda, K. E., Lee, D. J., and Lim, W. A. (1999) Structure of the enabled/VASP homology 1 domain-peptide complex: a key component in the spatial control of actin assembly. *Cell* **97,** 471–480
49. Lemmon, M. A., and Ferguson, K. M. (2000) Signal-dependent membrane targeting by pleckstrin homology (PH) domains. *Biochem. J.* **350,** 1–18
50. Treeck, M., Sanders, J. L., Elias, J. E., and Boothroyd, J. C. (2011) The phosphoproteomes of *Plasmodium falciparum* and *Toxoplasma gondii* reveal unusual adaptations within and beyond the parasites' boundaries. *Cell Host Microbe.* **10,** 410–419